Comparison of temperature dependent calibration methods of an instrument to measure OH and HO₂ radicals using laser-induced fluorescence spectroscopy

Frank A. F. Winiberg[1,2], William J. Warman[1], Charlotte A. Brumby[1], Graham Boustead[1], Iustinian G. Bejan[1,3], Thomas H. Speak[1], Dwayne E. Heard[1], Daniel Stone[1] and Paul W. Seakins[1]

[1] School of Chemistry, University of Leeds, Leeds, LS2 9JT, United Kingdom

[2] Now at: NASA's Jet Propulsion Laboratory, California Institute of Technology, Pasadena, 91109, USA

[3] Now at: Faculty of Chemistry and "Integrated Centre for Environmental Science Studies in the North-East Development Region – CERNESIM", "Al. I. Cuza" University of Iasi, Romania

Supplementary Information

Contents

S1 HIRAC Temperature Profiles

Figure S1(a) shows the square tubes that were welded to the side of the HIRAC chamber during construction. Every fourth tube was connected together to provide four separate circulation pathways to minimize pressure drops and temperature variations. The four pathways were connected to the thermostat unit (Huber 690W) via a inlet manifold (Figure S1(b)). The resultant temperature gradients are shown in Figure S2.
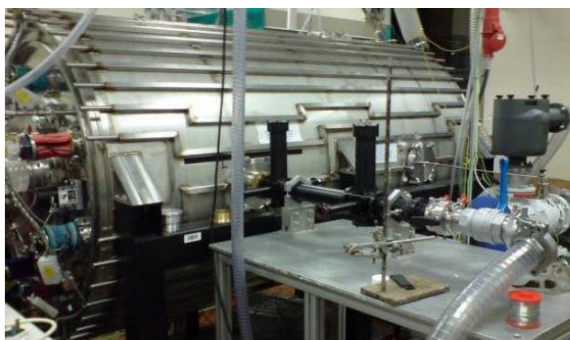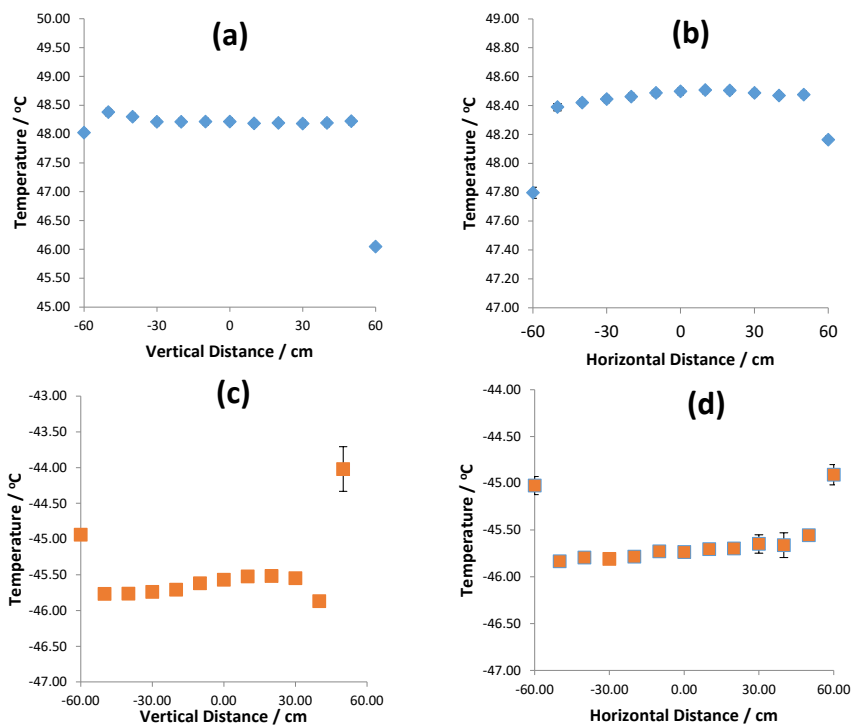

Figure S1(a): Square section tubing welded to the side of the HIRAC chamber

Figure S1(b): Inlet manifold to divert the fluid from the thermostat into 4 separate circulation pathways.


Figure S2: Temperature gradients measured across HIRAC at +48°C (a + b) and -46°C (c + d) at 1000 mbar.

1   **S2 Hydrocarbon Calibration Plots**

2   Accurate concentrations of the hydrocarbon(s) are required for the alternative calibration of

3   OH. Sequential additions of a known concentration of hydrocarbon were introduced into the

4   HIRAC chamber. The signal was measured on the mass spectrometer as shown in Figure S3a

5   for cyclohexane (monitored at m/z = 84.16 using N_2^+ as the ionization source). Figure S3b

6   shows the resulting calibration plot.

7
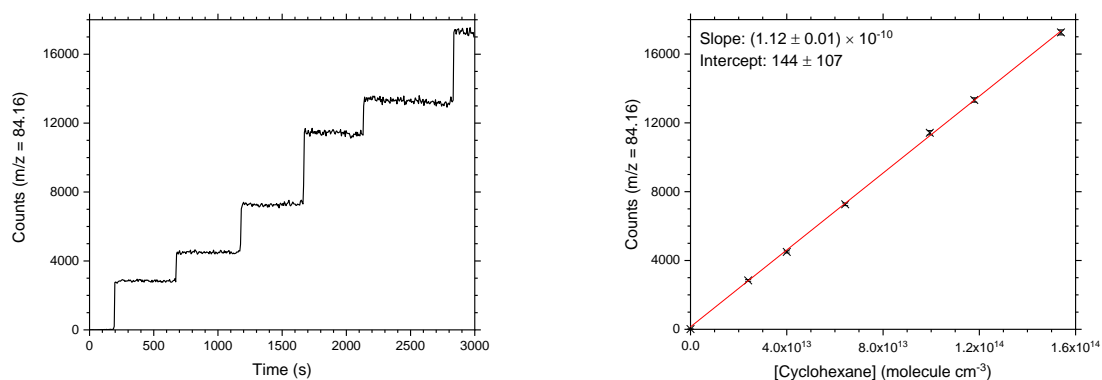
Figure S3(a): PTR signal as a function of additions of cyclohexane.
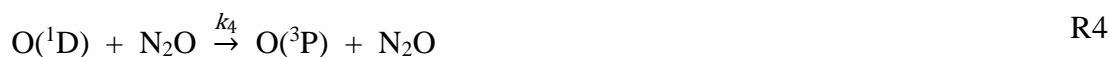
Figure S3(b): Corresponding calibration plot.

8

1   **S3 Further investigation of uncertainties in determination of $F_{184.9\ nm}$ for flowtube**

2   **calibration**

3   A schematic of the flowtube calibration set up is shown in Figure S4. The calculated [HOx] for

4   the conventional flowtube calibration is given by equation E2 of the main manuscript:

5 $$[OH] = [HO_2] = [H_2O]\ \sigma_{H_2O,\ 184.9\ nm}\ \Phi_{OH}\ F_{184.9\ nm}\ \Delta t \qquad (E2)$$

6   The uncertainties in the various components of E2 are given in Table 4 in the main text and it

7   can be seen that $F_{184.9\ nm}\ \Delta t$, the photon flux of the lamp is the major uncertainty. $F_{184.9\ nm}$ can

8   be determined in several ways, but most instruments use the photolysis of N_2O, with

9   measurement of the absolute amount of NO produced using a trace chemiluminescence

10   analyser as the method of choice. The reactions leading to NO are given below:

$$N_2O\ +\ h\nu\ \xrightarrow{k_1}\ N_2\ +\ O(^1D) \qquad\qquad R1$$

$$O(^1D)\ +\ O_2\ \xrightarrow{k_2}\ O(^3P)\ +\ O_2 \qquad\qquad R2$$

$$O(^1D)\ +\ N_2\ \xrightarrow{k_3}\ O(^3P)\ +\ N_2 \qquad\qquad R0$$

$$O(^1D)\ +\ N_2O\ \xrightarrow{k_4}\ O(^3P)\ +\ N_2O \qquad\qquad R4$$

$$O(^3P)\ +\ O_2\ +\ M\ \xrightarrow{k_5}\ O_3\ +\ M \qquad\qquad R5$$

$$O(^1D)\ +\ N_2O\ \xrightarrow{k_6}\ 2NO \qquad\qquad R6$$

$$O(^1D)\ +\ N_2O\ \xrightarrow{k_7}\ N_2\ +\ O_2 \qquad\qquad R7$$

11   Following the reactions described above, $F_{184.9\ nm}$ can be determined following equation ES1:

$$F_{184.9\ nm}\Delta t = \frac{(k_2[O_2] + k_3[N_2] + (k_7 + k_6)[N_2O])[NO]}{2(k_6 \sigma_{N_2O} \Phi_{O(^1D)}[N_2O]^2)} \qquad ES1$$

12   where Δt is the irradiation time which can be calculated from the known dimensions of the

13   "wand" as a function of the total flow rate of gas through the "wand", $\phi_{O(1D)}$ is the quantum

14   yield for the photodissociation $O(^1D)$ (~1) and σ_{N2O} is the absorption cross section of N_2O at

15   184.9 nm. σ_{N2O} is taken from the literature as $(1.43 \pm 0.02) \times 10^{-19}$ cm^2 molecule^{-1} (Creasey et

16   al., 2000). All the concentrations of species in ES1 are in molecule cm^{-3}.
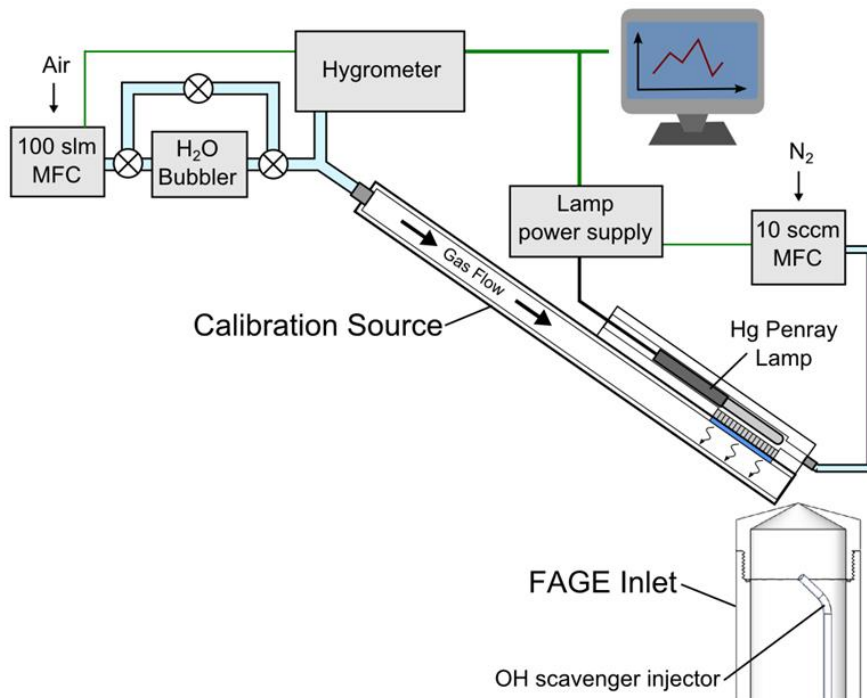
1

2   **Figure S4:** Schematic of flowtube calibration source.

3

4   Various experiments and procedures have been undertaken to check the reproducibility and

5   uncertainty in the determination of $F_{184.9\ nm}$.

6   (a) NOx analysers – Actinometry determinations require a measurement of the NO produced;

7   as [NO] is at relatively low levels, it is important to have an analyser of the appropriate

8   sensitivity. Chemiluminescence analysers will also show a small negative response to N_2O and

9   therefore it is important to calibration for this, see Figure S5a.

10

<div align="center">(a)   (b)</div>
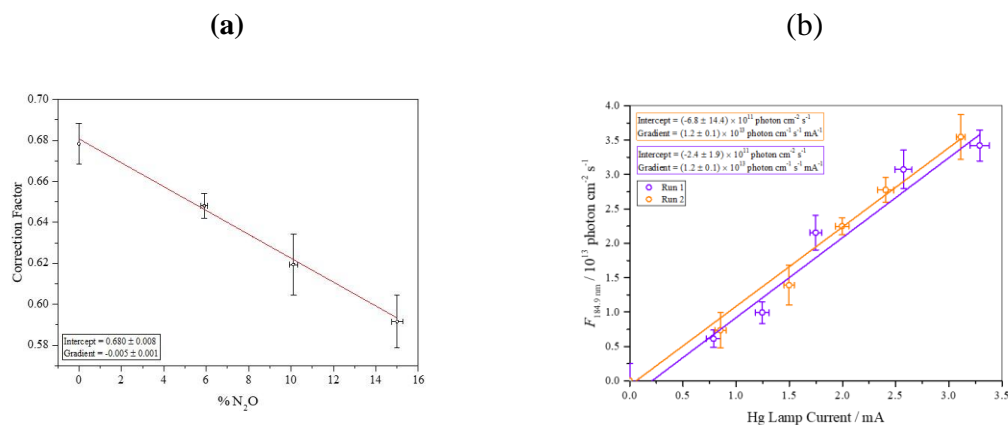
11   **Figure S5:** (a) Typical response of the NOx analyser calibration factor to N_2O. (b) Variation in
12   actinometry plot with N_2O passed through a Sofnofil trap (Run 1) and by-passing the trap (Run 2).

1 With regular calibration of the analysers the values of $F_{184.9\,nm}$ were within experimental error

2 for each of the analysers used.

3

4 (b) Impurities in the N_2O – Two actinometry calculations were undertaken passing or by-

5 passing the N_2O (BOC, medical grade) through a Sofnofil trap to remove NO and NO_2. As can

6 be seen in Figure S5(b) there is only a slight difference in the intercepts of the plot of $F_{184.9\,nm}$

7 vs lamp current (errors overlap) and no difference in the linearity of the plot.

8

9 (c) Lamp power supplies and software analysis – Actinometry plots produced identical

10 gradients and intercepts (within errors) with different lamp power supplies and with different

11 versions of software analysis.

12

13 Overall eight actinometry evaluations produced a mean value of $(1.07 \pm 0.09) \times 10^{13}$ photon

14 cm^{-1} s^{-1} mA^{-1} where the error is the 1σ statistical variation in the eight values. The overall

15 accuracy depends on the rate coefficients in equation ES1. These have undergone evaluations

16 by both IUPAC and JPL and despite extensive study have uncertainties in the region of 8 –

17 10%. Table S1 summarizes the various components of uncertainty in $F_{184.9\,nm}$.

18

19 **Table S1:** Contributions to uncertainties in $F_{184.9\,nm}$

Parameter	Uncertainty
Flows	2%
k_2	9%
k_3	8%
k_6	10%
k_7	10%
Precision	8%
$F_{184.9\,nm}$	**20%**

20

1 **S4 OH Relative rate plot to demonstrate removal by OH**

2 An important aspect to the alternative hydrocarbon analysis to determine OH sensitivity is that

3 the hydrocarbon is only chemically removed by OH and not any other oxidizing species. If

4 applicable first order dilution terms can be accounted for in the analysis. Figure S6 shows a

5 relative rate plot carried out under identical conditions to the hydrocarbon analysis, but with

6 no FAGE sampling and hence minimal dilution. The observed gradient of the plot 0.923 ±

7 0.010 (where the error in the gradient is statistical at the 2σ level), which represents the ratio

8 of the bimolecular rate coefficients, is in good agreement with the calculated literature ratio of

9 0.97 ± 0.14, where the error is based on a 10% error in each bimolecular rate coefficient.
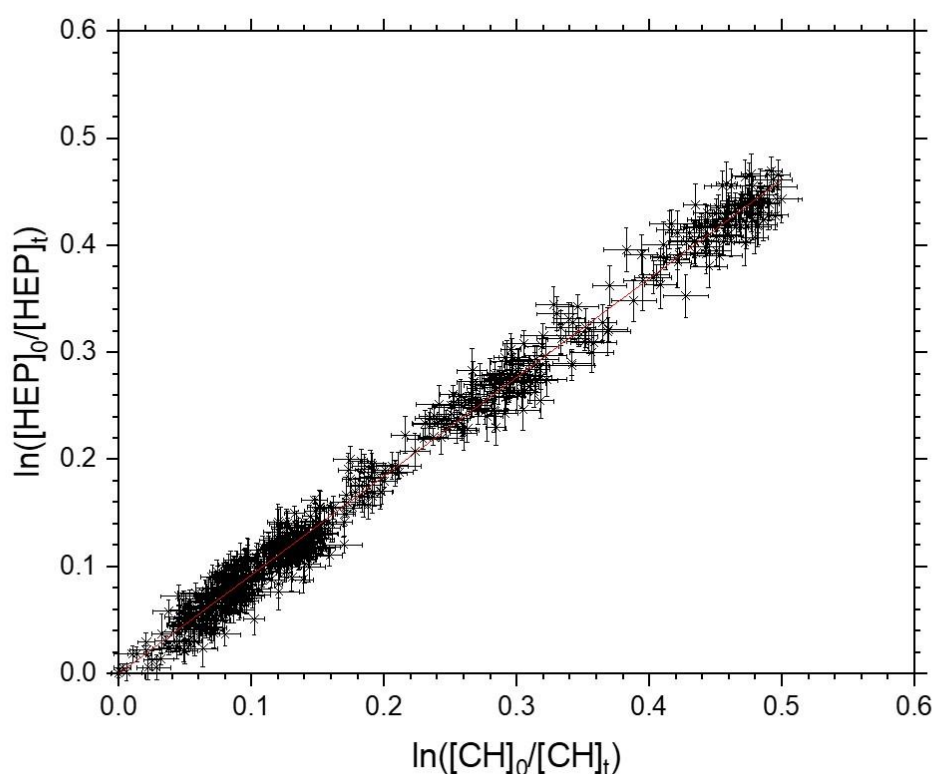
10

11 **Figure S6:** Relative rate plot of heptane (HEP) and cyclohexane (CH) to demonstrate that chemical
12 removal is consistent with removal by OH.

1 **S5 Temperature Dependence of Various Components of C_{HOx}**

2 The temperature dependence of the C_{HOx} factor depends on several factors as introduced in

3 the main text. These are: (1) Variation in the number density in the observation cell due to the

4 temperature difference between the gas in the observation cell and the gas temperature at

5 which [OH] is calculated, either in the flowtube or the HIRAC chamber. (2) Variation in

6 fluorescence quenching. Both the quenching rate coefficient and [Q] have a negative

7 temperature dependence, so that the fluorescence quantum yield will increase with increasing

8 temperature. (3) Variation in the relative population of the probed ro-vibrational state. (4)

9 Variation in the transmission of HOx through the FAGE pinhole and inlet tube. An estimate

10 of the losses through the flowtube could be estimated by looking at the variation in signal

11 with increased length of the inlet tube, but this would not account for losses at the pinhole.

12 HOx transmission through the pinhole and FAGE inlet is expected to show a positive

13 temperature dependence.

14 (a) Number Density

15 *Conventional calibration with calibration air at 293 K*

16 There is a decrease in the OH number density due to the change in pressure between the

17 sample, 1 bar, and the HOx cell, typically ~ 3 mTorr. However, this ratio will not be constant

18 over the variation in inlet temperature as the temperatures of the HOx cells will vary. The

19 correction factor, summarized for both OH and HO$_2$ cells in Table S2 is given by: $\frac{293}{T_{HOx}}$.

20

21 **Table S2:** Correction for change in number density relative to 293 K

T_{ext}/K	T_{OH}/K	Correction factor OH	T_{HO2}/K	Correction factor HO$_2$
266	279	1.043	284	1.025
276	285	1.021		
293	293	1.000	293	1.000
308	301	0.967	297	0.980
323	308	0.945	302	0.964
343	319	0.912	308	0.945

22

23 *Conventional calibration with calibration air matched to T_{Ext} via flowtube or HIRAC*

24 In these modes there is a smaller correction as the cell temperature is much closer to T_{Ext}, the

25 temperature at which [OH] is calculated either from the conventional flowtube calibration or

1 via the alternative kinetics based calibrations in the HIRAC chamber. The correction factor,

2 summarized in Tables S3 and S4, is given by: $\frac{T_{Ext}}{T_{HOx}}$.

3

4 **Table S3:** Correction for change in number density relative to T_{Ext} via flowtube calibration

T_{Ext}/K	T_{OH}/K	Correction factor OH	T_{HO2}/K	Correction factor HO_2
276	278	0.993		
278	280	0.993	287	0.969
293	293	1.000	293	1.000
323	320	1.009	301	1.073
343	338	1.015		

5

6 **Table S4:** Correction for change in number density relative to T_{Ext} via HIRAC calibrations

T_{Ext}/K	T_{OH}/K	Correction factor OH	T_{Ext}/K	T_{HO2}/K	Correction factor HO_2
273	276	0.989	273	286	0.955
293	293	1.000	293	293	1.000
323	320	1.009	308	297	1.037
348	341	1.021	323	302	1.070
			343	308	1.114

7

8 (b) Quenching and resultant changes in the fluorescence quantum yield

9 The degree of quenching of the excited OH will vary as a function of temperature. The

10 pseudo-first-order rate coefficient for OH quenching is given by $k_q[Q]$ where k_q is the

11 bimolecular rate coefficient for quenching by N_2 (dominant quencher) and [Q] is the number

12 density of the quenchers (N_2, O_2 and H_2O). Table S5 shows the variation in the quenching

13 parameters where the temperature dependence of k_q is taken from Bailey et al. (1999);Bailey

14 et al. (1997). The fluorescence quantum yield, Φ_f, is the ratio of the fluorescence rate

15 ($k_f[OH *]$) to the total rate of removal:

16 $$\Phi_f = \frac{k_f[OH*]}{k_f[OH*] + k_q[OH*][Q]} = \frac{k_f}{k_f + k_q[Q]} \qquad \text{ES2}$$

17 The relative change in the fluoresence quantum yield is shown in the last column of Table S5.

1   **Table S5:** Relative temperature dependence of parameters controlling Φ_f

T_{HOx}/K	[Q] rel	k_q rel	k' rel	Φ_f rel
281	1.036	1.034	1.071	0.948
285	1.021	1.021	1.042	0.968
290	1.003	1.005	1.008	0.994
295	0.986	0.988	0.975	1.020
300	0.970	0.972	0.943	1.046
310	0.939	0.940	0.882	1.100
317	0.918	0.917	0.842	1.139
330	0.882	0.875	0.772	1.214
338	0.861	0.849	0.731	1.262

2

3   (c) Relative population of Q

4   The final parameter which can be calculated is the relative strength of the initial absorption

5   due to the change in the rotational population of the ground electronic state probed by the

6     $Q_1(2)$ transition, which will vary with temperature. The relative rotational population, shown

7   in Table S6 was calculated with the LIFBase programme. There is a slight decrease in

8   population as temperature increases.

9

10   **Table S6:** Variation in rotational population of probed state $Q_1(2)$

T_{HOx}/K	Population (T)	Population relative to 293 K
280	0.206	1.035
284	0.204	1.025
293	0.199	1.000
310	0.193	0.970
323	0.187	0.940
340	0.181	0.910

11

12   The overall calculated temperature dependence relative to 293 K, will be the product of the

13   three correction factors. The calculated temperature dependences from the different

14   calibration methods where obtained by taking the product at the highest and lowest

15   temperatures and assuming a linear temperature dependence. The reported values are

16   presented in Table 6 of the main manuscript.

17

18   **S6 References**

19   Bailey, A. E., Heard, D. E., Paul, P. H., and Pilling, M. J.: Collisional Quenching of OH by N_2,
20   O_2 and CO_2, Journal of the Chemical Society, Faraday Transactions, 93, 2915-2920, 1997.

1 Bailey, A. E., Heard, D. E., Henderson, D. A., and Paul, P. H.: Collisional quenching of
2 OH($A^2\Sigma^+$, υ'=0) by H_2O between 211 and 294 K and the development of a unified model for
3 quenching, Chem. Phys. Lett., 302, 132-138, 1999.

4 Creasey, D. J., Heard, D. E., and Lee, J. D.: Absorption cross-section measurements of water
5 vapour and oxygen at 185 nm. Implications for the calibration of field instruments to measure
6 OH, HO_2 and RO_2 radicals, Geophysical Research Letters, 27, 1651-1654,
7 10.1029/1999gl011014, 2000.

8